Transactions of the Materials Research Society of Japan 30[1] 27-30 (2005)

Ferroelectricity and Electronic State of $(Sr,Ba)Nb_2O_6$ Thin Film Prepared on La-doped $SrTiO_3$ Substrate

Tohru Higuchi, Yoshiki Ebina, Takeshi Hattori and Takeyo Tsukamoto
Department of Applied Physics, Tokyo University of Science, 1-3 Kagurazaka, Shinjuku, Tokyo 162-8601, Japan
Fax: 81-3-5228-8241, e-mail: higuchi@rs.kagu.tus.ac.jp

The *c*-axis-oriented $Sr_{0.5}Ba_{0.5}Nb_2O_6$ (SBN) thin films were prepared on $La_{0.05}Sr_{0.95}TiO_3$ substrates by pulsed laser deposition. The *c*-axis orientation and grain size of the SBN thin films depend on substrate temperature (T_{sub}) during the deposition. When T_{sub} and Po_2 were fixed at 775°C and 7.5 mTorr, respectively, the SBN thin film exhibited a strong *c*-axis orientation and a smooth surface. The SBN thin film consisted of well-developed grains with a diameter of 200 nm. Its remanent polarization (P_r) and coercive field (E_c) were $2P_r$=32.1 μC/cm^2 and $2E_c$=135 kV/cm, respectively. The valence band and conduction band are composed of O 2*p* state and Nb 4*d* state, respectively. The energy separation between the top of the valence band and the bottom of the conduction band reflects the band gap of the SBN thin film. The band gap of this strongly *c*-axis oriented SBN thin film was approximately 3.1 eV, which accords with that of the SBN bulk crystal.

Key words: $Sr_{0.5}Ba_{0.5}Nb_2O_6$ (SBN), thin film, pulsed laser deposition, ferroelectricity, electronic state

1. INTRODUCTION

Ferroelectric $Sr_{1-x}Ba_xNb_2O_6$ exhibits a tetragonal tungsten-bronze crystal structure and has a spontaneous polarization along its *c*-axis [1]. Its ferroelectric properties, such as Curie temperature and dielectric constant (ε), can be adjusted by controlling the Sr/Ba atomic ratio in the range of $0.25 < x < 0.75$. $Sr_{1-x}Ba_xNb_2O_6$ is an attractive material for optoelectronic device applications because of its high electrooptic coefficient and strong photorefractive effect. Its figure of merit for photorefractive applications is more than 50 times higher than that of $LiNbO_3$. In addition, $Sr_{1-x}Ba_xNb_2O_6$ has a large spontaneous polarization and small ε that might be used for nonvolatile memory applications.

The $Sr_{1-x}Ba_xNb_2O_6$ thin films have been prepared by several fabrication techniques, such as sol-gel, pulsed laser deposition (PLD) and chemical solution deposition [2-10]. The *c*-axis orientation of the thin films has been already obtained at $SrTiO_3$ and MgO substrate [2-8]. In recent years, Sakamoto *et al.* has reported that the Gd, Er-doped $BaNb_2O_6$ thin films on Pt/MgO substrate exhibits a prominent *c*-axis preferred orientation and has a remanent polarization (P_r) of 7.0 μC/cm^2 [9-10], although the effect of leakage current is included. However, the good ferroelectricity of $Sr_{1-x}Ba_xNb_2O_6$ thin film has not been reported thus far.

In this study, we have prepared the *c*-axis oriented $Sr_{0.5}Ba_{0.5}Nb_2O_6$ (SBN) thin film on $La_{0.05}Sr_{0.95}TiO_3$ (LSTO) substrate by PLD and studied its electronic structure by X-ray absorption spectroscopy (XAS) and soft-X-ray emission spectroscopy (SXES). LSTO, which is one of the most typical perovskite-type oxides, has a metallic conductivity at room temperature. The lattice mismatch between SBN and LSTO was estimated to be approximately 5.0 %.

2. EXPERIMENTAL

SBN thin films were deposited on a (100)-oriented LSTO substrate by PLD using a SBN ceramic target. The single crystals of LSTO substrates, which were grown by the Czochralski method, were obtained from Furuuchi Kagaku Co., Ltd. The SBN ceramic target was prepared as follows: $SrCO_3$, $BaCO_3$ and Nb_2O_5 powders were mixed at a cation molar ratio of Sr:Ba:Nb = 0.5:0.5:2 using a wet ball mill. The mixture was pressed into a disk shape at 100kN and sintered for 4h at 1300°C. The target disk was polished to 21.3mm diameter and 4mm thickness. The target was examined using X-ray diffraction (XRD), as shown in Fig. 1. The density of SBN ceramic target was approximately 94 %.

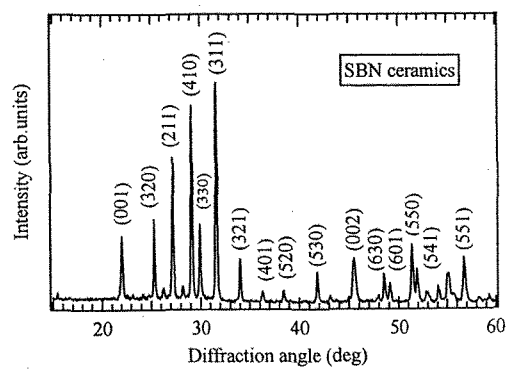

Fig. 1: XRD pattern of SBN ceramic target.

The PLD system was arranged in a symmetric configuration with a rotating substrate holder for compositional uniformity. The base pressure was ordinarily 9.0×10^{-9} Torr, and the substrate was inserted from a load lock chamber to maintain a low base

pressure. A KrF excimer laser (λ= 248 nm) was used for the ablation of the target. The laser power density and repetition frequency were 220 mJ/cm^2 and 9 Hz, respectively. The film thickness was fixed at approximately 400 nm. The top Pt electrodes with a diameter of 0.2mm were deposited on the film surface through a metal shadow mask by rf magnetron sputtering.

The structural properties were characterized by XRD analysis. The surface morphologies were observed by atomic-force-microscopy (AFM). The ferroelectricity was characterized using the ferroelectric property measurement system RT-6000HVS.

The electronic structure was characterized by SXES and XAS, which determine the electronic structure in the bulk state. The SXES and XAS were carried out in the revolver undulator beamline BL-19B at the Photon Factory of the High-Energy Accelerator Organization, Tsukuba, Japan. Synchrotron radiation was monochromatized using a varied-line spacing plain grating whose average groove density was 1000 lines/mm. The SXES spectrum was measured using a soft-X-ray emission spectrometer. The XAS spectrum was measured using a Si photodiode. The energy resolutions of SXES and XAS were approximately 0.4 eV and 0.1 eV, resepctively.

3. RESULTS AND DISCUSSION

Figure 2 shows the XRD patterns as a function of the substrate temperature (T_{sub}) for the SBN thin films. The oxygen gas pressure during the deposition was fixed at 7.5 mTorr. The (100) and (200) peaks of the LSTO substrates are observed at 2θ=22.8° and 46.7°, respectively. The (001) and (002) peaks of the SBN thin films are observed at 2θ=22.2° and 46.0°, respectively. The (410) peak is also observed at 2θ=29.5°. The SBN thin films prepared at T_{sub}=700°C does not exhibit the (001), (002), and (410) peaks, since the SBN thin films was not crystallized at 700°C. The intensities of (001) and (002) peaks increase at $T_{sub} \leq$ 775°C and decrease at T_{sub} > 775°C. Thus, the SBN thin film prepared at 775°C exhibits a strong *c*-axis orientation.

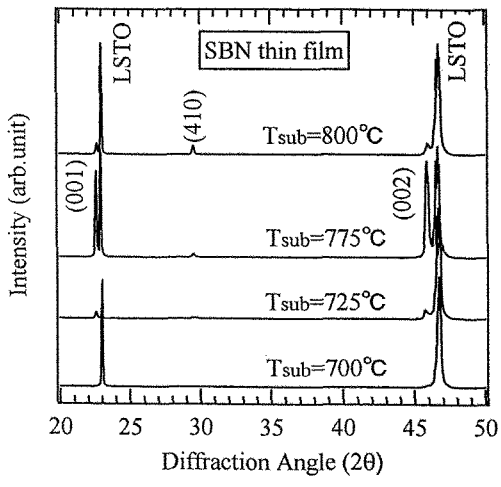

Fig. 2: XRD patterns as a function of T_{sub} in SBN thin films.

Figure 3(a) shows grain size as a function of T_{sub} for the SBN thin films. Grain size increases with increasing T_{sub}. In particular, the grain size at T_{sub}=800°C is equal to the film thickness. The large grain size might be originated from the three-dimensional islandlike crystal growth. The particles ablated from the target migrate on the heated substrate and form crystal nuclei at step or kinks on the substrate due to the large energy at the interface of the SBN thin film and the substrate.

Figure 3(b) shows the AFM image of the highly *c*-axis oriented SBN thin film prepared at T_{sub}=775°C. The SBN thin film consisted of well-developed grains with a diameter of 200 nm. Its surface roughness was approximately 20 nm against a film thickness of 400 nm. The SBN thin film was epitaxially growth with a *c*-axis perpendicular to the LSTO substrate.

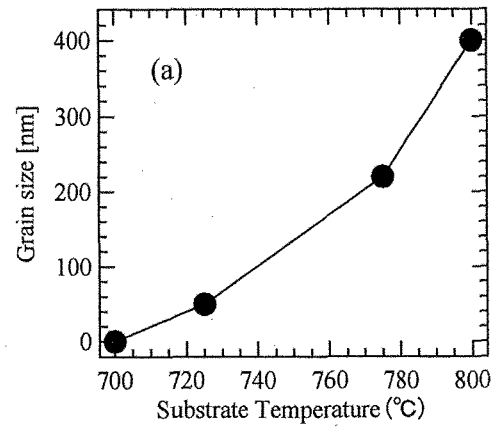

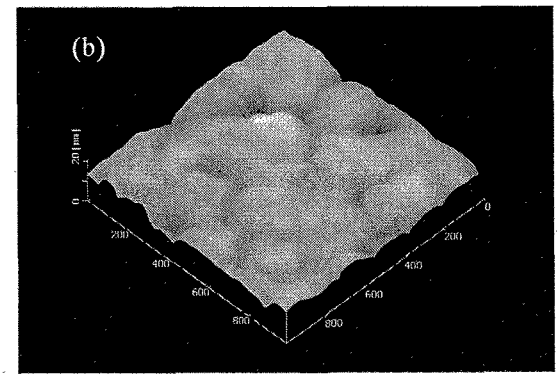

Fig. 3: (a) Grain size as a function of T_{sub} for SBN thin films. (b) AFM image of SBN thin film deposited at T_{sub}=775°C.

Figure 4 shows the hysteresis loops as a function of T_{sub} for the SBN thin films. The as-deposited SBN thin films did not exhibit ferroelectricity. Therefore, the as-deposited SBN thin films were annealed at 700~800°C in oxygen atmosphere for 1 h in order to investigate the effect of postannealing. The SBN thin film deposited at T_{sub}=700°C do not also exhibit ferroelectricity due to poor crystallization, as shown in Fig. 2. The SBN thin film deposited at T_{sub}=800°C is uniquely shape, which contributes to the large leakage current (>10^{-4} A/cm^2). A good *P-E* hysteresis loop of the SBN thin film is observed at T_{sub}=775°C. Then, the

P_r and coercive field (E_c) were $2P_r$=32.1 μC/cm^2 and $2E_c$=135 kV/cm, respectively. The ε was approximately 160. These values are superior to those of the SBN thin films obtained by sol-gel and chemical solution deposition methods [6-10]. The good ferroelectricity of the highly *c*-axis oriented SBN thin film at T_{sub}=775°C contributes to the relatively small grain size and the smooth surface, as shown in Fig. 3(b).

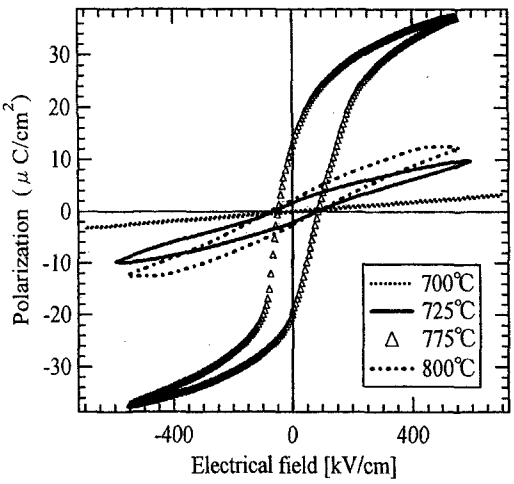

Fig. 4: *P-E* hysteresis loops as a function of T_{sub} for SBN thin films.

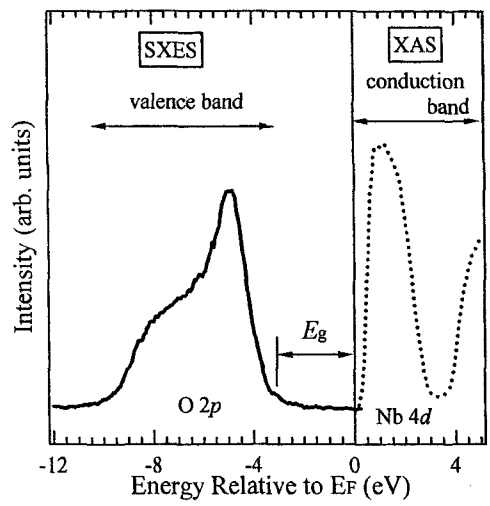

Fig. 5: O 1s SXES and XAS spectra of *c*-axis oriented SBN thin film. The SXES and XAS spectra reflect the electronic structures of valence band and conduction band, respectively.

Figure 5 shows the O 1*s* SXES and XAS spectra of the *c*-axis-oriented SBN thin film deposited at T_{sub}= 775°C. The bottom axes of the SXES and XAS spectra are normalized by the binding energy of the O 1*s* photoemission peak. The clear selection rule of SXES occurs mainly within the same atomic species, because the core hole is strongly localized [11]. For this reason, the O 1*s* SXES spectrum reflects the O 2*p* partial density of state (PDOS). The obtained O 2*p* PDOS corresponds to the electronic structure in the valence band region, because the valence band of SBN is mainly composed of O 2*p*. On the other hand, from the dipole selection rule, it is understood that the O 1*s* XAS spectrum of Nb oxide corresponds to transitions from the O 1*s* state to the O 2*p* state. The large absorption band at approximately 1.5 eV is mainly composed of the unoccupied Nb 4*d* state hybridized with the O 2*p* state. The energy separation between the top of the O 2*p* valence band and the bottom of the Nb 4*d* conduction band reflects the band gap. The band gap of the *c*-axis-oriented SBN thin film is estimated to be approximately 3.1 eV.

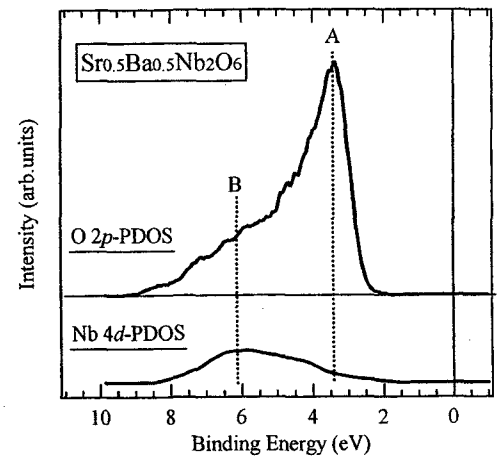

Fig. 6 Comparison of O 1*s* and Nb 4*p* SXES spectra in the valence band region of $Sr_{0.5}Ba_{0.5}Nb_2O_6$ thin film.

Figure 6 shows the Nb 4*p* and O 1*s* SXES spectra in the valence band region of the SBN thin film. The intensity of each spectrum is normalized to beam current and measurement time. The Nb 4*p* SXES spectrum measured at *hv*=65 eV reflects the Nb 4*d*-PDOS in the valence band region. The contributions of the Sr 4*d* and Ba 5*d* bands were not observed in the valence band region. Thus, the sum of the O 2*p* PDOS and Nb 4*d* PDOS is the total DOS in the valence band of the SBN thin film.

The Nb 4*d* PDOS has a broad distribution on the left side of feature B. The Nb 4*d* PDOS contribution is more significant at high binding energies (feature B), where the O 2*p* state has a larger admixture with the Nb 4*d* state. That is, the valence states originating from the O 2*p* state are hybridized with the Nb 4*d* state. From the distributions of the Nb 4*d* PDOS and O 2*p* PDOS, we consider that feature A corresponds to the nonbonding state and feature B corresponds to the bonding state that is well mixed with the Nb 4*d* state. The hybridization effect between the Nb 4*d* and O 2*p* states in Nb oxide has not been reported to date. However, a similar hybridization effect has been observed in $4d^0$ metal transition oxides, such as ZrO_2 and $CaZrO_3$ [12,13]. In perovskite-type oxide $CaZrO_3$, it was reported that the contribution of Zr 4*d* PDOS is more significant at high binding energies in the valence band region, where the bonding O 2*p* state has a larger admixture with the Zr 4*d* state. The contribution of the

Zr 4*d* PDOS to the total DOS has been reported to be approximately 25% in the valence band [12]. For the $Sr_{0.5}Ba_{0.5}Nb_2O_6$ thin film, the contribution of the Nb 4*d* PDOS, which was estimated from the total DOS, was approximately 20 % in the valence band.

4. CONCLUSION

We prepared the highly *c*-axis oriented SBN thin film on LSTO substrate by PLD method and studied its electronic structure using SXES and XAS. The structural and ferroelectric properties of SBN thin films were dependent on Po_2 and T_{sub} during deposition. When the Po_2 and T_{sub} were fixed at 7.5 mTorr and 775 °C, respectively, the SBN thin film exhibited a highly *c*-axis oriented SBN single phase. The *c*-axis oriented SBN thin film consisted of well-developed grains and exhibited a good *P-E* hysteresis loop. Then, P_r and E_c were $2P_r$=32.1 μC/cm^2 and $2E_c$=135 kV/cm, respectively. The band gap of this strongly *c*-axis oriented SBN thin film was approximately 3.1 eV, which accords with that of the SBN bulk crystal. The O 1*s* and Nb 4*p* SXES spectra exhibited the O 2*p* PDOS and Nb 4*d* PDOS, respectively, in the valence band. The energy position of the O 2*p* state overlaps with that of the Nb 4*d* state, indicating that the O 2*p* state hybridizes with the Nb 4*d* state in the valence band. The contribution of the Nb 4*d* PDOS to the total DOS was estimated to be approximately 20% in the valence band.

ACKNOWLEDGEMENTS

We would like to thank Mr. M. Sogawa for his useful discussion. This work was partially supported by the Grant- In-Aid for Scientific Research from the Ministry of Education, Culture, Sports, Science and Technology.

REFERENCES

[1] P. B. Jamieson, S. C. Abrahams and J. L. Bernstein: J. Chem. Phys. **48** (1968) 5048.
[2] C. J. Chen, Y. Xu, R. Xu and J. D. Mackenzie: J. Appl. Phys. **69** (1991) 1763.
[3] S. Hirano, T. Yogo, K. Kikuta and K. Ogiso: J. Am. Ceram. Soc. **75** (1992) 1697.
[4] K. Tanaka, O. Nakagawa, M. Nakano, T. Shimuta, H. Tabata and T. Kawai: Jpn. J. Appl. Phys. **37** (1998) 6142.
[5] M. Nakano, H. Tabata, K. Tanaka, Y. Katayama and T. Kawai: Jpn. J. Appl. Phys. **36** (1997) L1331.
[6] S. S. Thony, K. E. Youden, J. S. Harris and L. Hesselink: Appl. Phys. Lett. **65** (1994) 2018.
[7] W. J. Lin, T. Y. Tseng, S. P. Lin, S. L. Tu, S. J. Yang, J. J. Harn, K. S. Liu and I. N. Lin: Jpn. J. Appl. Phys. **34** (1995) L625.
[8] H. F. Cheng, C. T. Hu and I. N.Lin: Jpn. J. Appl. Phys. **36** (1997) 284.
[9] W. Sakamoto, Y. Horie, T. Yogo and S. Hirano: Jpn. J. Appl. Phys. **40** (2001) 5599.
[10] W. Sakamoto, M. Mizuno, T. Yamaguchi, K. Kikuta and S. Hirano: Jpn. J. Appl. Phys. **42** (2003) 5913.
[11] N. Ohtake, T. Higuchi, K. Ando, A. Fukishima, S. Shin and T. Tsukamoto: Jpn. J. Appl. Phys. **43** (2004) 7627.
[12] T. Higuchi, T. Tsukamoto, Y. Tezuka, K. Kobayashi, S. Yamaguchi and S. Shin: Jpn. J. Appl. Phys. **39** (2000) L133.
[13] C. Morant, A. Fernandez, A. R. Gonzalez-Elipe, L. Soriano, A. Stampfl, A. N. Bradshaw and I. M. Sanz: Phys. Rev. B **52** (1995) 11711.

(Received December 23, 2004; Accepted January 31, 2005)